Title

Microcircuit Mechanisms through which Mediodorsal Thalamic Input to Anterior Cingulate Cortex Exacerbates Pain-Related Aversion

Journal

Neuron, 102(5)

ISSN

0896-6273

Authors

Meda, Karuna S
Patel, Tosha
Braz, Joao M
et al.

Publication Date

2019-06-01

DOI

10.1016/j.neuron.2019.03.042

Peer reviewed

Published in final edited form as:

Neuron. 2019 June 05; 102(5): 944–959.e3. doi:10.1016/j.neuron.2019.03.042.

Microcircuit mechanisms through which mediodorsal thalamic input to anterior cingulate cortex exacerbates pain-related aversion.

Karuna S. Meda[1], **Tosha Patel**[2], **Joao M. Braz**[1], **Ruchi Malik**[2], **Marc L. Turner**[2], **Helia Seifikar**[2], **Allan I. Basbaum**[1], and **Vikaas S. Sohal**[2,3]

[1]Department of Anatomy and Kavli Institute for Fundamental Neuroscience, University of California, San Francisco, 94143

[2]Department of Psychiatry, Weill Institute for Neurosciences, and Kavli Institute for Fundamental Neuroscience, University of California, San Francisco, 94143

[3]Lead contact

SUMMARY

Hyperexcitability of the anterior cingulate cortex (ACC) is thought to drive aversion associated with chronic neuropathic pain. Here we studied the contribution of input from mediodorsal thalamus (MD) to ACC, using sciatic nerve injury and chemotherapy-induced mouse models of neuropathic pain. Activating MD inputs elicited pain-related aversion in both models. Unexpectedly, excitatory responses of layer V ACC neurons to MD inputs were significantly weaker in pain models compared to controls. This caused the ratio between excitation and feedforward inhibition elicited by MD input to shift towards inhibition, specifically for subcortically-projecting (SC) layer V neurons. Furthermore, direct inhibition of SC neurons reproduced the pain-related aversion elicited by activating MD inputs. Finally, both the ability to elicit pain-related aversion, and the decrease in excitation, were specific to MD inputs; activating basolateral amygdala inputs produced opposite effects. Thus, chronic pain-related aversion may reflect activity changes in specific pathways, rather than generalized ACC hyperactivity.

eTOC blurb

Meda et al. show that in chronic pain states, mediodorsal thalamic (MD) inputs to anterior cingulate cortex (ACC) undergo pathway-specific changes. As a result, MD-ACC inputs suppress

Corresponding Authors: Dr. Allan Basbaum (allan.basbaum@ucsf.edu) and Dr. Vikaas Sohal (vikaas.sohal@ucsf.edu).

Author Contributions:

KM, AB, and VS designed the experiments and wrote the manuscript. KM performed behavioral experiments with help from TP and HS. MT performed additional behavioral experiments. KM performed the physiology experiments except for the voltage clamp recordings using strontium, which RM performed. R.M also helped with current clamp recordings. JB performed spared nerve injury surgeries and Taxol injections. KM and VS analyzed the data.

Declaration of Interests: The authors declare that they have no competing financial interests.

the activity of many subcortically-projecting ACC neurons, thereby driving negative pain-related affect.

INTRODUCTION

Chronic pain affects roughly 25% of the population, with the needs of many patients unmet by current therapies (Bouhassira et al., 2008; Breivik et al., 2006). While much is known about the neural basis of the sensory-discriminative aspects of pain (Basbaum et al., 2009; Fernandez and Turk, 1992; Melzack and Casey, 1968), attention has recently turned to mechanisms underlying the affective dimension of pain, especially the role of the anterior cingulate cortex (ACC) (Vogt 2005; Tracey and Mantyh, 2007; Johansen et al., 2001). In humans, the ACC is activated by acutely painful stimuli (Casey, 1999), and tonically hyperactivated in chronic pain (Moisset and Bouhassira, 2007; Price, 2000; Treede et al., 1999; Apkarian et al., 2001). Manipulations that selectively decrease the perceived unpleasantness, but not the intensity, of a painful stimulus, are associated with reduced ACC activity, without concurrent changes in somatosensory cortex (Rainville et al., 1997). Cingulotomy was an early surgical intervention for intractable pain, after which patients reported decreased unpleasantness of their pain, even though the sensory-discriminative aspects remained intact (Hurt and Ballantine, 1973; Folt and White, 1963). In rodents, ACC lesions significantly reduce aversion produced by intraplantar injection of formalin or mechanical stimulation of an injured paw (Johansen et al., 2001; LaGraize et al., 2004). ACC lesions also block conditioned preference elicited by analgesic drugs in animals with ongoing neuropathic pain (King et al., 2009; Qu et al., 2011).

Despite this strong evidence implicating the ACC in pain-related aversion, remarkably little is known about how inputs from other brain regions engage ACC circuits. This study focuses on inputs from the mediodorsal thalamus (MD). MD afferents terminate most densely in layer V of the ACC (Krettek and Price, 1977; Musil and Olson, 1988; Kuroda et al., 1998; Berendse and Groenewegen, 1991), where pyramidal neurons responding to noxious stimuli also reside (Yamamura et al., 1996). The MD receives nociceptive inputs from the spinal cord (Giesler et al., 1979; Cliffer et al., 1991), the medullary subnucleus reticularis dorsalis (Villanueva et al., 1991; Villanueva et al., 1998) and the pontine parabrachial nucleus (Bester et al., 1999). The MD and neighboring medial thalamic nuclei are the major source of nociceptive information to the ACC (Dong et al., 1978; Hsu et al., 1997, Yang et al., 2006). Importantly, lidocaine injections into or lesions of medial thalamic nuclei block nociceptive responses of ACC neurons (Hsu et al., 1997, Hsu et al., 2000). Both ACC and MD demonstrate long latency responses to nociceptive stimuli, with large, bilateral receptive fields and little somatotopic organization (Dong et al., 1978, Sikes and Vogt, 1992). This is consistent with the MD encoding features of pain affect and transmitting them to the ACC. In fact, imaging and electrophysiological studies in patients and animal models demonstrated that the MD, like the ACC, is hyperactivated in chronic pain (Rinaldi et al, 1991; Mao et al, 1993; Whitt et al., 2013).

Here, we directly test the hypothesis that MD input to ACC contributes to chronic pain-related aversion. We find that optogenetic activation of MD inputs to the ACC elicits

aversion in both nerve injury and chemotherapy-induced models of neuropathic pain. Dissecting the underlying circuit mechanisms, we find that MD input elicits excitation as well as feedforward inhibition in layer V ACC pyramidal neurons. In models of neuropathic pain, this response shifts towards inhibition, specifically within subcortically-projecting (SC) pyramidal neurons. Furthermore, direct optogenetic inhibition of SC neurons replicates the behavioral effect of MD input activation: pain-related aversion. These results point to a novel circuit mechanism through which MD-ACC inputs influence pain-related aversion. Strikingly, these findings are specific to the MD-ACC pathway; we found the opposite pattern of behavioral and synaptic changes when we examined basolateral amygdala (BLA) inputs to ACC. Thus, our study shows how a specific input-output pathway through the ACC undergoes unexpected alterations that are conserved across two models of neuropathic pain, and contribute to chronic pain-related aversion.

RESULTS

Activating MD inputs to the ACC exacerbate pain-related aversion

We studied how activating MD inputs affects pain-related aversion using a conditioned place preference (CPP) paradigm (Figure 1A) that measures ongoing aversiveness associated with chronic neuropathic pain (Qu et al., 2011). We used both traumatic nerve injury and chemotherapy-induced models of neuropathic pain. In both models, mice show conditioned place preference for gabapentin (Park et al, 2013; Bannister et al, 2017; Juarez-Salinas et al, 2018), which is the first-line clinical therapy for neuropathic pain (Colloca et al, 2017). Taken together with the fact that ACC lesions block preference for gabapentin in both models (Johansen et al, 2001; Qu et al, 2011), we conclude that in both models, mice experience pain and the ACC is a critical mediator of pain-related aversion. To activate excitatory inputs to the ACC, we injected an adeno-associated virus (AAV5) that drives expression of a channelrhodopsin-2 (ChR2)-eYFP fusion protein under control of the CaMKIIα promoter into MD, then implanted an optical fiber over ACC (Figure 1B). To model the chronic neuropathic pain condition we performed spared nerve injury (SNI) or injected Taxol 3 weeks after viral injection and optical fiber implantation. CPP was performed 7–10 days after the SNI procedure or Taxol injection, allowing 4–5 weeks for viral expression (Figure 1B). In this assay, the effect of the conditioning stimulus can be quantified by a “preference score” for the stimulated side, i.e., the % time spent on the stimulated side on the post-test day (relative to the total time spent on the stimulated and unstimulated side), normalized by the % time spent on the same side on the pre-test day (again, relative to total time on the stimulated and unstimulated sides). Comparing the time spent on the stimulated side on the pre-test (i.e. pre-conditioning) day, to the time spent on the same side on the post-test (i.e., post-conditioning) day controls for inherent variability in preferences. Normalizing by the total time spent on either the stimulated or unstimulated side further controls for potential differences in the total amount of exploration on the two days. Stimulation that exacerbates pain-related aversion should produce a preference score significantly < 1 in animals with chronic pain, but not in pain-free controls. Conversely, stimulation that attenuates pain-related aversion should elicit a preference score significantly > 1 in animals with chronic pain, but not in pain-free controls. After conditioning, animals with chronic neuropathic pain avoided the chamber paired with optogenetic activation of

MD inputs, indicated by a preference score significantly < 1 (SNI, 0.86 ± 0.07; Taxol, 0.90 ± 0.04). Pain-free animals neither preferred nor avoided the stimulated side, i.e., their preference score was not significantly different from 1 (Control, 1.18 ± 0.16; Saline, 1.03 ± 0.09) (Figure 1C). This same conclusion could be reached by analyzing "difference scores," i.e., the difference in the amount of time an animal spends in a chamber on the test vs. pretest days (Figure S1A and B). ANOVA on the difference (test minus pre-test) in time spent on the stimulated or unstimulated side showed a significant interaction between side (stimulated vs. unstimulated) and condition (pain: SNI/Taxol vs. no pain: control/saline) ($p = 0.016$), but no main effect of condition ($p = 0.71$) or side (stimulated vs. unstimulated, $p = 0.07$), and no interaction between experiment type (SNI vs. Taxol), side and condition ($p = 0.35$). Thus, activating MD inputs to ACC exacerbates pain-related aversion.

Optogenetically activating MD terminals could potentially elicit back-propagating action potentials in MD neurons which project to ACC. Therefore, we used optogenetic inhibition to confirm that the behavioral effects of activating MD inputs reflect local actions within ACC. We carried out these experiments using the same timeline as before, but now inhibited MD inputs to ACC using archaerhodopsin (Arch) driven by a Synapsin promoter (AAV5-hSyn-eArch-eYFP) (Figure 1D). Indeed, Arch-mediated inhibition of MD inputs elicited effects opposite to those of activating MD inputs, i.e., animals with pain developed a preference for the chamber paired with optogenetic inhibition, indicated by a preference score significantly > 1 (SNI, 1.61 ± 0.28). Interestingly, we observed a preference for optogenetic inhibition of MD inputs in pain-free controls as well (preference score significantly > 1, Control, 1.22 ± 0.10) (Figure 1E). Again, analyzing difference scores supported the same conclusion (Figure S1C). Thus, inhibiting MD inputs to ACC shows that these inputs transmit an aversive signal. Optogenetic activation of MD inputs is sufficient to elicit conditioned aversion in mice with chronic neuropathic pain, but not in control mice, suggesting that the aversive signal transmitted by MD inputs to ACC is enhanced in the setting of chronic pain. The enhancement of this aversive signal may be explained by changes in how MD input recruits ACC neurons in control vs. pain conditions. Subsequent experiments explore this possibility.

Importantly, control experiments confirmed that light delivery and virus injection alone into MD (expression of eYFP only) did not elicit conditioned preference or aversion in animals with chronic neuropathic pain, i.e., the preference score was not significantly different from 1 (SNI, 1.00 ± 0.21) (Figure S2A).

Excitatory responses of layer V ACC neurons elicited by MD inputs are significantly weakened in the setting of chronic neuropathic pain

We hypothesized that the ability of MD input activation to exacerbate pain-related aversion might reflect cellular and/or synaptic changes within the ACC. Blom et al (2014) found that layer V ACC pyramidal cells are hyperexcitable in a chronic nerve ligation model of neuropathic pain. That study did not distinguish pyramidal cell subtypes described for layer V of ACC and adjacent medial prefrontal cortex (mPFC) (Dembrow et al., 2010; Gee et al., 2012). One subtype projects to subcortical structures including MD (Figure 2A, B). In these subcortically-projecting (SC) cells, the hyperpolarization-activated cation current (I_h)

produces a prominent voltage sag and afterdepolarization in response to a hyperpolarizing current pulse (Figure 2C and D). The second subtype of intratelencephalically-projecting (IT) neurons, which target the contralateral cortex, has a much less pronounced sag and afterdepolarization (Figure 2C and D). Using these physiological characteristics to identify the IT and SC subtypes, we studied their intrinsic properties in slices of the rostral ACC (Figure 2E) using whole-cell patch clamp (Figure 2F and G). As Figure 2H shows, in slices from SNI and Taxol animals, both subtypes became hyperexcitable, as indicated by a significant increase in the F/I slope compared to neurons from pain-free animals (Control IT, 1.35 ± 0.06 vs. SNI IT, 1.57 ± 0.07; Control SC, 1.11 ± 0.06 vs. SNI SC, 1.47 ± 0.06. Saline IT, 1.35 ± 0.06 vs. Taxol IT, 1.61 ± 0.10; Saline SC, 1.11 ± 0.06 vs. Taxol SC, 1.40 ± 0.11). There was no change in the resting membrane potential or input resistance of either IT or SC neurons in the setting of pain, compared to control (Figure S3).

Next we asked whether MD inputs to the ACC, specifically to IT or SC neurons, are altered in the setting of chronic neuropathic pain. To evaluate this, we again used AAV5-CaMKII-ChR2 virus to express ChR2-eYFP in MD-ACC projections (Figure 3A, B). MD axons in ACC terminate in layer I and superficial layer V (Figure 3C). To activate MD inputs, we delivered blue light flashes through a 40X objective while recording voltage clamp responses from IT or SC neurons (Figure 3D). Traces of the population average of excitatory post-synaptic currents (EPSCs) evoked by 5 Hz stimulation are shown in Figure 3E and G. Surprisingly, the peak EPSC amplitudes elicited by stimulation of MD inputs were dramatically reduced in both IT and SC neurons from both SNI and Taxol animals compared to pain-free, controls (Control IT, −1312 ± 148 pA vs. SNI IT, −785 ± 119 pA; Control SC, −1087 ± 129 pA vs. SNI SC, −334 ± 124 pA. Saline IT, −1293 ± 177 pA vs. Taxol IT, −759 ± 170 pA; Saline SC, −723 ± 160 vs. Taxol SC, −253 ± 60 pA) (Figure 3F and 3H). In fact, despite the fact that both IT and SC neurons exhibit increased intrinsic excitability in the setting of pain, current clamp recordings (Figure 3I) showed that the probability of spiking in response to activation of MD inputs was markedly reduced in IT and SC cells from SNI animals compared to uninjured controls: Control IT, 0.98 ± 0.02 vs. SNI IT, 0.79 ± 0.07; Control SC, 0.97 ± 0.02 vs. SNI SC, 0.10 ± 0.06) (Figure 3J). Taxol treated animals exhibited a similar reduction in IT cell spiking (Control IT, 0.87 ± 0.06, n=19 cells vs. SNI IT, 0.61 ± 0.10, n=14 cells; $p<0.05$, unpaired t-test). SC cells spiked at negligible levels in both Taxol and control mice (Figure 3K).

Interestingly, excitatory responses of IT cells to MD input activation were significantly greater than those of SC cells, in both animals with pain and controls (Two-way ANOVA using cell type and pain vs. control condition as factors and including an interaction term). Thus MD inputs to ACC preferentially excite IT neurons, and are weakened in animals with pain (either SNI or Taxol) in both IT and SC neurons.

To investigate whether the weakening of MD-evoked EPSCs observed in the setting of pain reflects pre- vs post-synaptic mechanisms, we measured the paired-pulse ratio (PPR) between the second and first EPSCs in the 5Hz train represented in Figure 3E. Examining either SC or IT neurons, we didn't find a significant difference in PPR for the Control vs. SNI or Saline vs. Taxol conditions (Figure S4A, B), suggesting that changes in MD-evoked EPSCs may reflect post-synaptic mechanisms.

To more strongly establish a pre- vs. post-synaptic locus for changes in MD-evoked EPSCs, we recorded asynchronous unitary EPSCs (uEPSCs) elicited by optogenetically stimulating MD terminals after replacing calcium in the external solution with strontium (Sr^{2+}, 2 mM) (Figure S4C). There was no difference in the average uEPSC frequency between SNI and Control (Control: 16.7 ± 0.3, n=11 cells vs. SNI: 16.7 ± 0.2). By contrast, we noticed a marked shift in the distribution of uEPSCs towards lower amplitudes in the SNI group (Figure S4D). Indeed, when we performed ANOVA on the number of small (< 6pA) vs. medium-large (> 6pA) uEPSCs in each cell, we found a significant interaction between uEPSC amplitude and condition (SNI vs. control) ($p<0.05$), confirming that this change in the amplitude distribution is statistically significant. By contrast, there was not a significant main effect of condition, i.e., there was not an overall change in the number of uEPSCs in the SNI vs. control condition, consistent with our finding that the uEPSC frequencies did not differ. Interestingly, when we plotted the number of small uEPSCs vs. the number of medium/large uEPSCs, we observed a negative linear relationship, with SNI cells shifted towards more small uEPSCs and fewer medium-large uEPSCs (Figure S4E).

Chronic neuropathic pain shifts the E/I ratio elicited by MD inputs towards inhibition in SC cells

We also measured feedforward perisomatic inhibition evoked by MD inputs in IT and SC neurons, by recording in voltage clamp at +10 mV while optogenetically activating MD inputs (Figure 4A). Traces of the population average of feedforward inhibitory post-synaptic currents (IPSCs) evoked by 5 Hz stimulation are shown in Figure 5B. In contrast to the marked reduction in EPSCs elicited by activating MD inputs in the setting of chronic pain, feedforward IPSC amplitudes were not significantly different for SNI or Taxol compared to controls (Figure 4B,C). In particular, whereas reductions in EPSC amplitude were statistically significant for both SC and IT cells in both the SNI and Taxol models, none of these comparisons were significant for feedforward IPSCs (Control IT, 1029 ± 209 vs. SNI IT, 811 ± 116; Control SC, 885 ± 172 vs. SNI SC, 685 ± 182. Saline IT, 1790 ± 186 vs. Taxol IT, 1450 ± 345; Saline SC, 1047 ± 266 vs. Taxol SC, 1308 ± 252). For IPSCs in IT cells from SNI mice, the reduction in IPSC amplitude approached significance ($p=0.052$, unpaired t-test), but were not significant when we pooled together all of the IPSC data and performed ANOVA with cell type, condition, and pain model as factors.

Consistent with our finding that feedforward IPSCs were relatively intact in animals with pain, we also found that EPSCs recorded from fast-spiking interneurons (Figure S5A) did not differ between SNI and Control animals (Control: −785 ± 186 vs. SNI: −904 ± 186) (Figure S5B). We didn’t find a significant difference in PPR between SNI and Control (Figure S5C). In conclusion, we found no evidence for disinhibition in the responses of layer V ACC pyramidal neurons to MD input in the setting of chronic pain.

Given that we observed consistent and marked reductions in EPSC amplitudes, but more modest and inconsistent reductions in IPSCs, we explicitly tested whether the relative levels of excitation to inhibition (E:I ratio) elicited by MD-ACC inputs were altered in the setting of pain. For each cell we calculated E:I ratios based on the EPSCs and IPSCs measured during responses to MD input activation. Specifically, 1 ms light pulses had been used to

evoke EPSCs, whereas 5ms pulses were used for feedforward inhibition. A ratio of 1 does not imply perfectly "balanced" excitation and inhibition because EPSCs and IPSCs were recorded at different holding potentials and using different light pulse durations to optimize each set of measurements. Rather, comparing E:I ratios reveals whether decreases in synaptic excitation are larger than those in synaptic inhibition, when measured using a common set of cells from control and pain conditions. Indeed, the E:I ratio for synaptic responses elicited by MD input activation was significantly smaller for animals with pain (i.e., shifted towards inhibition) than for controls ($p < 0.05$, significant main effect of condition by ANOVA using pain vs. control, SNI vs. Taxol models, and cell type as factors) (Figure 4D). This effect was present across both SNI and Taxol models. However, the ANOVA did reveal a significant interaction between condition (pain vs. control) and cell type (IT vs. SC) ($p < 0.05$). Indeed, when examined separately, the E:I ratio was significantly reduced for SC (Control SC, 0.91 ± 0.24 vs. SNI SC, 0.37 ± 0.09; Saline SC, 0.82 ± 0.23 vs. Taxol SC, 0.24 ± 0.10) but not IT neurons (Control IT, 0.57 ± 0.14 vs. SNI IT, 0.48 ± 0.10; Saline IT, 0.45 ± 0.13 vs. Taxol IT, 0.43 ± 0.13) (Figure 4D). This difference likely reflects the strong trend that we observed towards reduced IPSCs in IT neurons.

This finding suggested that the net influence of MD input on SC neurons becomes less excitatory and more inhibitory in a chronic pain setting. To corroborate this finding, we recorded spiking from SC neurons in response to depolarizing current injection, with or without concurrent optogenetic activation of MD input (Figure 5B). Representative traces are shown in Figure 5A. In Control mice, MD input increased spiking in all SC neurons (13/13 cells), i.e., there were significantly more spikes during Light ON than in the Baseline condition (Baseline, 17.2 ± 2.5 vs. Light ON, 22.9 ± 2.2) In contrast, in the SNI and Taxol conditions, activating MD input did not consistently increase SC neuron spiking (SNI, Baseline, 20.8 ± 3.1 vs. Light ON, 20.7 ± 3.2; Taxol, Baseline, 19.6 ± 2.8 vs. Light ON, 20.5 ± 2.5) (Figure 5C). In fact, in 4/11 SNI SC neurons and 6/13 Taxol SC neurons, activating MD inputs actually reduced spiking (Figure 5D). This adds further evidence that the net effect of MD input activation on SC neurons shifts towards inhibition in the setting of chronic neuropathic pain.

Inhibiting SC neurons in ACC exacerbates pain-related aversion

Taken together, our results suggest that in animals with chronic neuropathic pain, activating MD inputs can actually *reduce* the activity of some SC neurons. By contrast in control conditions, activating MD inputs consistently excites SC neurons. This difference occurs because in animals with pain, MD inputs preferentially recruit feedforward inhibition, which in turn, suppresses responses to excitatory input (Figure 6A). This model predicts that direct inhibition of SC neurons should replicate the behavioral effect of MD input activation, that is, elicit aversion in animals with chronic pain (Figure 6B). To test this, we measured the effects of inhibiting SC neurons within the ACC in mice with chronic neuropathic pain (Taxol) or pain-free controls. In these experiments, we injected canine adenovirus that encodes Cre (CAV2-Cre virus) into the MD thalamus, which, along with other subcortical structures like the periaqueductal grey, is a major target of SC neurons (Collins et al., 2018). Thus, when we refer to "SC neurons," we are generally referring to MD-projecting neurons. This virus traffics retrogradely to the ACC, where we injected a YFP-tagged virus to drive

Cre-dependent Arch expression (Figure 6D). At the end of the experimental (Figure 6C), we confirmed that SC neurons in the infragranular layers of ACC were YFP+ (Figure 6E). Consistent with the predictions of the model outlined above, animals with chronic neuropathic pain (but not saline-treated controls) spent less time on the side paired with optogenetic inhibition of SC neurons, i.e., they had a preference score significantly < 1 (Taxol: 0.78 ± 0.09) (Figure 6F). The same conclusion is reflected in the difference score (Figure S1F). We also confirmed that the aversion elicited by inhibiting SC neurons occurs specifically in Taxol-treated mice by performing ANOVA on the change in time (test minus pre-test) spent on the stimulated or unstimulated side after inhibiting SC neurons in Taxol or saline-treated mice. This ANOVA showed a significant interaction between side (stimulated vs. unstimulated) and condition (Taxol vs. saline) ($p = 0.00002$), but no main effect of condition ($p = 0.34$) or side ($p = 0.40$). In other words, inhibiting SC neurons exacerbated pain-related aversion and replicates the behavioral effect of activating MD inputs to the ACC.

We also used the same strategy to activate SC neurons by injecting Cre-dependent ChR2 in ACC (Figure S6A, B) and found a trend towards preference in both control (1.2 ± 0.1) and Taxol animals (1.24 ± 0.14) (Figure S6C, S1H). Direct activation of SC neurons will affect multiple downstream targets, which may explain why we observed only a trend towards preference elicited by activation of SC neurons in animals with chronic pain.

We also studied the effect of inhibiting IT neurons, by injecting the CAV2-Cre virus in contralateral ACC and Cre-dependent Arch in the side of the optical fiber (Figure 6G). Neither control animals nor those with chronic neuropathic pain preferred or avoided the side paired with IT neuron inhibition, i.e., their preference scores were not significantly different from 1 (Saline, 1.30 ± 0.16; Taxol, 1.07 ± 0.21) (Figure 6H, S1G). This finding underscores the importance of monitoring activity in distinct populations of ACC neurons, and suggests that the SC subpopulation specifically contributes to chronic pain-related aversion.

This model also explains effects of BLA input on pain-related aversion

The preceding results raise two questions. First, is the decreased ability of MD inputs to excite ACC neurons in a chronic pain condition specific to the MD-ACC pathway, or are other inputs similarly affected? Second, does our model in which reduced activity of SC neurons drives chronic pain-related aversion predict the effects of other inputs to the ACC? To address these questions, we carried out parallel studies focusing on basolateral amygdala input to ACC.

The BLA is densely and reciprocally connected with both the ACC and MD (Sarter and Markowitsch, 1983; McDonald 1991; Hoover and Vertes, 2007; Musil and Olson, 1988, Velayos et al., 1985). BLA has been heavily implicated in aversive learning and pain-related aversion (Helmstetter and Bellgowan, 1992; LeDoux 2000). Similar to ACC lesions, lesions of the BLA abolish conditioned aversion to intraplantar formalin and noxious footshock (Gao et al., 2004; Tanimoto et al., 2003). Infusion of an NMDA antagonist or morphine into the BLA also reduces formalin-induced conditioned place aversion (Deyama et al., 2007).

Finally, BLA lesions inhibit the chronicity of pain following peripheral nerve injury (Li et al., 2013).

We measured responses of IT and SC neurons in ACC to BLA input (Figure 7A). In contrast to the pain-related decrease in MD input to SC neurons, EPSCs evoked by optogenetic activation of BLA inputs in animals with chronic neuropathic pain were significantly *increased* compared to control (Control SC, −78 ± 10 pA vs. SNI SC: −181 ± 27 pA; Saline SC, −121 ± 27 pA, vs. Taxol SC: −265 ± 55 pA). Notably, this increase was not significant in IT cells for either the SNI or Taxol conditions (Control IT, −120 ± 23 pA vs. SNI IT: −140 ± 14; Saline IT: −81 ± 22 pA vs. Taxol IT: −189 ± 65) (Figure 7B and C). For IT neuron responses to BLA input, the paired-pulse ratio (PPR) between the second and first EPSCs in a 5Hz train did not differ between either pain model and the corresponding control. However, for SC neurons from SNI animals there was a large and significant *increase* in PPR (Control SC, 0.87 ± 0.09 vs. SNI-SC: 1.46 ± 0.17). We observed a similar trend for SC neurons in the Taxol model (Saline SC, 1.10 ± 0.08 vs. Taxol SC: 1.47 ± 0.22) (Figure S7). This suggests that changes in pre-synaptic function may occur for BLA inputs to SC neurons in the setting of chronic pain, although these changes in pre-synaptic function would likely not explain the observed strengthening of these connections (which would typically be associated with increased probability of release and thus reduced PPR). In both control and pain conditions, activation of of BLA-ACC inputs elicited feedforward inhibitory responses in IT and SC neurons and EPSCs in inhibitory interneurons that were very small and often not quantifiable. Also unlike MD inputs, which preferentially excited IT cells, BLA inputs recruited SC and IT cells equally (ANOVA using cell type, pain vs. control, and SNI vs. Taxol models as factors and including an interaction term between cell type and condition).

Based on the model outlined above, where MD input to SC neurons shifts in the inhibitory direction in models of chronic pain, while excitatory BLA inputs to SC neurons are potentiated, BLA input should become a major contributor to SC neuron activity in the setting of chronic neuropathic pain. Thus, by exciting SC neurons, activating BLA inputs might reduce inhibition of SC neurons, and elicit conditioned preference in animals with chronic neuropathic pain. It follows that inhibiting BLA inputs should strongly decrease the excitation to SC neurons, producing conditioned aversion in a chronic pain setting.

We tested these predictions, using the SNI model 4 weeks after injection of AAV5-CaMKII-ChR2 virus into BLA and implantation of an optical fiber in ACC. We measured CPP 7–10 days after SNI, allowing 5–6 weeks for viral expression (Figure 8A, B). In marked contrast to MD inputs, optogenetic activation of BLA inputs to the ACC elicited conditioned preference (preference score significantly > 1) in both control animals (Control, 1.19 ± 0.08) and mice with chronic neuropathic pain (SNI, 1.49 ± 0.23) (Figure 8C). Difference scores reflect the same changes in Figure S1D. Next, we optogenetically inhibited BLA inputs to the ACC (Figure 8D). Strikingly, *inhibiting* BLA inputs to the ACC elicited behaviors identical to those seen when we *activated* MD inputs: aversion (preference score significantly < 1) in animals with chronic neuropathic pain (SNI, 0.79 ± 0.07), but not in control animals (0.94 ± 0.09) (Figure 8E). Difference scores reflect the same conclusion (Figure S1E). We also performed ANOVAs on the changes (test minus pre-test) in time spent on the stimulated side in SNI vs. control animals. In this case, we saw a main effect of

side (stimulated vs. unstimulated, p = 0.024), but no significant effect of group (p = 1) or side X group interaction (p = 0.29). Thus, this particular dataset (which may be underpowered for this between-group comparison) does not support a between-group difference. Regardless, this experiment shows that activating BLA vs. MD inputs elicits different effects (preference vs. aversion, respectively) in animals with pain. A control experiment confirmed that light delivery and virus injection alone into BLA (driving expression of eYFP only) did not elicit conditioned preference or aversion in nerve-injured animals (Figure S2B).

DISCUSSION

Here we used optogenetics to activate a major input to ACC – the mediodorsal thalamus (MD) – and uncovered an input-output pathway that contributes to pain-related aversion. Activating MD inputs elicited conditioned place aversion in mice with chronic neuropathic pain, but not controls. To identify physiological changes within the ACC that may drive these behavioral effects, we examined IT and SC layer V neurons. Both are hyperexcitable in chronic pain, but unexpectedly, their excitatory responses to MD input decreased significantly in both the SNI and Taxol models of chronic pain. Moreover, in SC neurons, the ratio of excitation to inhibition elicited by MD input actually shifted towards inhibition in the setting of pain. Consistent with a model in which MD input exacerbates pain-related aversion by inhibiting SC neurons, direct inhibition of SC neurons elicits the same behavioral effect as activating MD inputs: conditioned aversion, specifically in animals with pain. These findings provide insight into mechanisms through which a specific input-output pathway, involving MD inputs and SC neurons, contributes to pain-related aversion. Importantly, although we have studied one pathway, there are likely to be others which represent important subjects for future studies. In particular, we also examined how BLA-ACC input is altered and contributes to pain-related aversion. Strikingly, we observed pathway-specific changes: whereas MD-ACC excitation was weaker in animals with pain, BLA-ACC excitation grew stronger. Consistent with the idea that this makes BLA input an important driver of SC neurons in animals with pain, and that decreases in SC neuron activity contribute to pain-related aversion, inhibiting BLA inputs elicited aversion specifically in animals with pain.

All of these physiological abnormalities were conserved across two different models of chronic pain. This reinforces the idea that the divergent plasticity of the MD-ACC and BLA-ACC pathways is a key factor in chronic pain, rather than an idiosyncratic feature of one model. Importantly, whereas SNI affects one side of the body, Taxol produces generalized pain; thus, the fact that the same changes occur in both models suggests that these are general rather than lateralized features of the pain state.

This study describes the preference / aversion induced by a total of 16 distinct experimental conditions. While most of these results are internally consistent, we do observe some asymmetric effects of optogenetic excitation and inhibition, e.g., in control mice stimulating MD inputs has no effect, whereas inhibiting them elicits conditioned preference. This is not entirely surprising, since inhibition suppresses endogenous patterns of activity whereas optogenetic excitation imposes potentially non-physiological patterns of activity, and

inhibition only affect cells which are already active, whereas excitation tends to activate all cells (Phillips and Hasenstaub, 2016). Nevertheless, through this large number of experiments, we have achieved multiple independent confirmations of the key aspects of our model: in animals with pain, MD input to SC neurons shifts in the direction of inhibition, and inhibiting SC neurons is aversive. As a result, in pain models, exciting MD inputs exacerbates pain-related aversion in both SNI and Taxol-treated animals, whereas inhibiting MD inputs ameliorates this aversion. These four observations, representing our core results, are all internally consistent.

A circuit model for pain-related aversion

We propose a model that diverges significantly from many existing ones, which propose that overall ACC activity drives pain aversion. Specifically, (1) we found no evidence for disinhibition of layer V ACC circuits in chronic pain; (2) we did not find evidence that hyperactivity of either IT or SC neurons contributes to chronic pain (because we inhibited both populations, and in neither case did this elicit conditioned preference); (3) we found that activating different inputs to the ACC elicits opposing effects on pain-related aversion, arguing against the idea that exciting the ACC invariably drives chronic pain-related aversion; (4) we found that activating BLA input to the ACC elicits conditioned preference, at odds with prevailing views of BLA-ACC inputs as mainly aversive.

Of course, we do not mean to imply that hyperexcitability within the ACC plays no role in pain-related aversion or hyperalgesia. In both the SNI and Taxol models, individual SC and IT neurons become hyperexcitable, and BLA input to ACC is potentiated. However, even though SC neurons become hyperexcitable, their responses to synaptic input from MD thalamus becomes weaker in the pain state. Furthermore, increases in BLA input to ACC do not seem to contribute to pain-related aversion. Thus, while we expect that hyperexcitability within certain ACC pathways likely contributes to pain-related aversion, our findings suggest that these contributions must be understood in a cell-type and circuit-specific manner. A related point is that we specifically examined aversion in the chronic pain state, and the circuits we studied may play different roles with respect to hyperalgesia and/or acute responses to pain.

Previous studies examined the role of MD in pain using lesions or pharmacology. Such approaches do not allow the study of specific MD connections. In fact, lesion studies of the MD and pain-related aversion have been largely inconclusive due to differences in the size and location of lesions, as well as the variable atrophy of surrounding target structures (Wang et al., 2007; Li et al., 2004; Chai et al., 2010). Electrophysiological studies face similar limitations. Although brain sections can preserve the thalamocingulate pathway, electrical stimulation activates fibers of passage and axon collaterals, confounding the specificity of evoked ACC responses. Our study used optogenetics to overcome some of these limitations. While we found that the influence of MD input on SC neurons in ACC becomes more inhibitory in the setting of pain, it is unclear whether this would tonically reduce SC activity vs. prevent the MD input from increasing SC activity at specific moments, etc. Future studies might explore this by simultaneously monitoring SC neuron activity and MD-ACC input while measuring pain-related aversion in behaving mice.

Feedforward inhibition mediated by cortical inhibitory interneurons (Agmon and Connors, 1991; Swadlow, 2002; Swadlow, 2003) is a key feature of thalamocortical interactions, thought to control the temporal precision of cortical responses to sensory stimuli. MD inputs directly innervate inhibitory interneurons in the ACC, particularly those expressing parvalbumin (PV), and silencing ACC PV interneurons prolongs MD-evoked EPSCs in ACC pyramidal neurons (Delevich et al., 2015). Conceivably, this inhibition regulates temporal integration by SC neurons. Indeed, it has been shown that activating MD inputs elicits powerful inhibitory gating of hippocampal-evoked firing of layer V pyramidal neurons in the neighboring mPFC (Floresco and Grace, 2003).

MD and ACC may form a recurrent excitatory loop. Ultrastructural studies demonstrate that thalamocortical axon terminals from MD make direct excitatory synapses onto the dendrites of ACC pyramidal neurons which project back to MD (Kuroda et al., 1993a). High frequency electrical stimulation of MD can evoke long latency spikes in ACC, likely via the antidromic activation of ACC axons that project to MD (Pirot et al., 1994). Thus, the increased inhibition of SC neurons we observed in the chronic pain condition may disrupt the transmission of relevant affective and nociceptive information through this loop. Recurrent activity in similar MD-prefrontal loops has been shown to play critical roles in cognitive tasks (Bolkan et al., 2017; Schmitt et al., 2017, Guo et al., 2017).

IT cells can integrate cortical processing across hemispheres whereas SC cells are positioned to exert top-down control over subcortical structures. As a result, IT and SC neurons can differentially modulate affective processing by recruiting distinct downstream networks. We found that whereas inhibiting SC neurons elicits aversion in animals with pain, but not in controls, inhibiting IT neurons results in neither aversion nor preference in either animals with pain or controls.

Limitations and future directions

We still do not understand the downstream mechanism(s) through which SC neuron inhibition elicits pain-related aversion, but at least two possibilities should be considered. One arises from the fact that a population of SC neurons in the ACC likely projects to the periaqueductal grey (PAG), a region strongly implicated in mechanisms of pain relief (Young et al., 1997; Fardin et al., 1987). In the setting of chronic pain, increased inhibition of SC-PAG projecting neurons could suppress excitatory drive to the PAG, thereby reducing its antinociceptive actions and exacerbating the aversiveness of a chronic pain state. Alternatively, collaterals of SC neurons may target GABAergic inhibitory interneurons in subcortical structures. As a result, suppressing the activity of SC neurons could disinhibit a target driving aversion, e.g., the lateral habenula (Matsumoto and Hikosaka, 2009; Stamatakis and Stuber, 2012).

If SC neurons in the ACC are part of a descending pain-modulatory circuit that becomes engaged in the setting of chronic pain, then stimulating or inhibiting SC neurons might be expected to suppress or exacerbate responses to painful stimuli in mouse models of chronic pain. This study has focused on the affective, rather than sensory, aspects of chronic pain. However, future studies could measure how optogenetically manipulating SC neurons affects acute pain thresholds using the von Frey or tail flick tests.

Conclusions

Our findings suggest that activity in specific ACC input-output pathways, rather than the overall level of ACC activity, underlies the contribution of the ACC to pain-related aversion. It follows that therapeutic interventions which preferentially target specific inputs to ACC (e.g., from MD thalamus) or selective populations of ACC neurons (e.g., SC neurons) may be more effective for treating the affective components of chronic pain than nonspecific interventions aimed at suppressing overall ACC activity.

STAR METHODS

CONTACT FOR REAGENT AND RESOURCE SHARING

Further information and requests for resources and reagents should be directed to and will be fulfilled by the Lead Contact, Vikaas Sohal (vikaas.sohal@ucsf.edu).

EXPERIMENTAL MODEL AND SUBJECT DETAILS

All experiments were performed with male C57BL/6J mice (Simonsen Laboratory). Animals were group-housed under standard conditions with *ad libitum* access to food and water. Injections were performed at 3–4 weeks of age and either electrophysiology or behavior experiments were conducted at 8–10 weeks of age. For all electrophysiology experiments all animals were housed under a standard 12 hr light/dark cycle. For behavioral experiments conducted in red light, animals were housed under a reverse 12 hr light/dark cycle for 3 days prior to and for the duration of the experiment. Littermates were randomly assigned to experimental groups. Sample sizes were chosen based on effect sizes from previous experiments. All experiments were conducted in accordance with procedures established by the Administrative Panels on Laboratory Animal Care at the University of California, San Francisco.

METHOD DETAILS

Slice preparation—We cut 250 μm coronal slices from 8 to 10-week-old male C57BL6 mice (Gee et al., 2012). Slices were cut in a chilled slicing solution in which Na+ was replaced by sucrose, then incubated in warmed artificial cerebrospinal fluid (ACSF) at 30°C–31°C for ~1 hr before being used for recordings. ACSF contained 126 mM NaCl, 26 mM NaHCO3, 2.5 mM KCl, 1.25 mM NaH2PO4, 1 mM MgCl2, 2 mM CaCl, and 10 mM glucose. We secured the slice by placing a harp along the midline between the two hemispheres.

Intracellular recording—We obtained somatic whole-cell patch recordings from visually identified pyramidal cells in layer V of rostral anterior cingulate cortex using differential contrast video microscopy on an upright microscope (BX51WI; Olympus). Recordings were made using a Multiclamp 700A (Molecular Devices). Except when otherwise noted, patch electrodes (tip resistance = 2–6 MOhms) were filled with the following (in mM): 130 K-gluconate, 10 KCl, 10 HEPES, 10 EGTA, 2 MgCl, 2 MgATP, and 0.3 NaGTP (pH adjusted to 7.3 with KOH). All recordings were at 32.5±1°C. Series resistance was usually 10– 20 MΩ, and experiments were discontinued above 30 MΩ. Fast-spiking interneurons were

identified based on their electrophysiological properties, i.e., narrow action potentials, high maximal firing rates and minimal accommodation.

Voltage clamp recordings—To record EPSCs, we held cells at −70 mV and recorded responses to MD inputs evoked by 1.0 ms light pulses. 1.0 ms was chosen as the optimum pulse width, as we observed that excitation evoked by MD inputs was so strong that sometimes unclamped spikes were elicited even in voltage clamp. To record feedforward inhibition, we held the same cells at +10 mV and recorded responses to 5.0 ms light pulses. In contrast to excitation, 1.0 ms light pulses were not strong enough to evoke responses and thus 5.0 ms light pulses were determined to be optimum to evoke feedforward inhibition. Unitary postsynaptic events in Sr^{2+} containing ACSF were recorded in voltage-clamp mode. 100 flashes were delivered with 12 sec in between. Events were collected for 700 ms starting 200 ms after each flash. Unitary EPSCs were detected off-line using Clampfit (pClamp, Molecular devices) event detection.

Current clamp recordings—To record the effect of MD input activation on spiking, we recorded neurons in current clamp mode with the same intracellular solution. In a separate experiment to identify MD-evoked inhibition of SC neurons, we again recorded in current clamp mode, whereby we delivered a 1.0 sec current pulse (starting at 50 pA and increasing in 50 pA steps), a 1.0 sec gap, and then a second current pulse. 20 Hz, 1.0 ms blue light flashes came on 100 ms before the second current pulse and turned off at the end of the second current pulse. There was a 10 sec delay before the next sweep.

Stereotactic surgeries—Injections were performed using standard mouse stereotactical methods. Mice were anesthetized for the duration of the surgery using 2% isofluorane gas. After cleaning with Betadiene and ethanol, a midline incision was made in the scalp. The skull was leveled, and small burr holes were drilled over the brain region of interest using a dental drill. Virus was injected through a 10ul Hamilton syringe using a microinjector (World Precision Instruments) at a speed of 100–150 nL/minute and the scalp was closed using tissue adhesive (Vetbond). For injections into MD thalamus, coordinates were (in millimeters relative to bregma): −1.7 A/P, +0.3 M/L, and −3.43 D/V. For injections into the BLA, coordinates were (in millimeters relative to bregma): −1.34 A/P, +3.11 M/L, and −4.74 D/V. For injections into the ACC, coordinates were (in millimeters relative to Bregma): +1.50 A/P, 0.26 M/L (contra- and ipsilateral), −1.50 and −1.75 D/V. For behavior experiments, animals were implanted with a chronic unilateral custom-made 200 μm optical fiber (Doric Lenses) targeted to the ACC (+1.51 A/P, +0.25 M/L, −1.13 D/V, in millimeters relative to Bregma). All injections and implants were performed in 3–4 week old male C57BL6 animals, and preparation of brain slices or behavior experiments were conducted 4–6 weeks later.

Viral expression of optogenetic proteins—All adeno-associated viruses (AAV) were designed in the Deisseroth Lab and purchased from UNC Vector Core. We expressed channelrhodopsin (ChR2) in terminals from either MD or BLA using an AAV5 vector that contains a gene encoding ChR2-eYFP under control of the CaMKIIα promoter. We expressed archaerhodopsin from either MD or BLA terminals using an AAV5 vector that

contains a gene encoding eArch3.0-eYFP under the control of the Synapsin promoter. A virus containing eYFP alone under control of the CaMKII promoter was used as a control virus. To label subcortically projecting (SC) neurons or intratelecephalic (IT) neurons, we used the CAV2-Cre virus from BioCampus in conjunction with a Cre-dependent Arch-eYFP or ChR2-eYFP virus into the ACC. For virus injections in MD or BLA, 0.35 μl of virus was injected at a rate of 100 nl/min. For injections into the ACC, 0.60 μl of virus was injected at a rate of 150 nl/min. For post-hoc verification of CAV2-Cre virus injections, histology focused on confirming that we observed the expected pattern of labeling in the ACC. For example, when labeling SC neurons via CAV-cre injections into MD, we confirmed that we observed sparse labeling that was restricted to deep layers, similar to what we observed following injections of retrogradely transported fluorescent beads into MD

***In vitro* optogenetic stimulation—**We activated ChR2 in either MD or BLA terminals using flashes of light generated by a Lambda DG-4 high-speed optical switch with a 300W Xenon lamp, and an excitation filter set centered around 470 nm, delivered to the slice through a 40X objective (Olympus). Illumination was delivered across a full high-power (40X) field.

***In vivo* optogenetic stimulation—**We connected mice to a optical patch cable (Doric Lenses) 2 days before the experiment each day for 30–60 min to habituate them to the tethering procedure. Following the tethering procedure, we ran mice in the behavioral procedure (see below). For channelrhodopsin stimulation experiments, we used a 10 mW laser with a stimulation frequency of 20 Hz and a 5.0 ms light pulse duration for all behavioral experiments (controlled by a function generator Agilent 33210A Series Arbitrary Waveform Generator). Total light power for all experiments was 5–10 mW. For archaerhodopsin experiments, we delivered continuous stimulation at a power of 2–2.5 mW.

Retrograde labeling—For retrograde labeling of IT and SC cells, we injected Alexa-Fluor conjugated cholera toxin beta-subunit (AF-CTB) 488 nm and 594 nm (Invitrogen) into the MD thalamus and contralateral cortex. For injections in MD, 0.35 μl was injected at a rate of 100 nl/min. For injections into the ACC, 0.50 μl was injected at a rate of 100 nl/min.

Neuropathic pain models—Chemotherapy (Taxol)-induced neuropathy and the spared nerve injury (SNI) model were used. Four intraperitoneal injections (i.p) of Taxol (Sigma, diluted in 40% dimethyl sulfoxide saline) at a dose of 1mg/kg were made every other day. Control animals received saline injections. In the SNI model, the tibial branch of the sciatic nerve was isolated and spared, and then 8–0 silk suture (Ethicon) was used to ligate the sural and common peroneal branches of the sciatic. Next the ligated branches were transected distal to the ligature and 2–4 mm of each distal nerve stump removed. Overlying muscle and skin layers were closed separately with 6–0 silk and staples (Harvard Apparatus). Because we previously demonstrated that sham-operated animals manifest some “pain-related” behaviors, presumably secondary to the limited nerve injury produced during the sham surgery (Urban et al., 2011), in the present study control animals had no surgery. For all physiology experiments, the experimenter had a colleague kill the animal so that experimenter was blind to the eartag and genotype (pain or no pain) before slicing. For all

behavior experiments, a colleague did all of the Taxol and SNI surgeries respectively and the code was broken at the time of data analysis. Each cage of mice included both experimental and control mice.

Conditioned Place Preference—The conditioned place preference (CPP) apparatus (Tap Plastics) consists of a three-chambered box, a left chamber with vertical black and white stripes on the wall and a punched metal floor, a middle neutral chamber with grey walls and a smooth floor, and a right chamber with black and white spots on the wall and a mesh floor. The CPP test consists of 4 days. Day 1 is the Pre-Test Day in which mice have access to all three chambers, and we record the time spent in each chamber. On days 2 and 3, animals are restricted to either the left or right chamber (counterbalanced across all mice) and receive either 5.0 ms flashes of blue light at 20 Hz (stimulation) for 20 min, or no stimulation for 20 min. Approximately 4 hours later, the mice are restricted to the opposite chamber and receive the other treatment (stimulation or no stimulation). 24h after the last conditioning session on Day 4 – Test Day – the mice again have access to all three chambers, and time spent in each chamber is recorded. On Pre-test and Test Day, the animal's movement was tracked using ANYmaze software. We calculated a Preference Score for the stimulated chamber (Preference for Stim Side - the ratio of the time spent in the stimulated side on Test day to Pre-Test day. We also calculated a Difference Score (The time spent in the stimulated chamber on Pre-Test day subtracted from the time spent in that chamber on Test day). Animals were not used if they spent more than 75% of total time spent in one chamber on Pre-Test day.

QUANTIFICATION AND STATISTICAL ANALYSIS

Data were analyzed using custom-written Matlab scripts (MathWorks). All statistical computations were performed using GraphPad Prism 7.0 software. Statistical significance was accepted at the level $p < 0.05$. We used student's t-test to compare pairs of groups if data were normally distributed (verified using Lillie test). If more than two groups were compared, we used ANOVA with post-hoc tests between groups corrected for multiple comparisons (Holm-Sidak or Bonferroni). Data are represented in the figures as mean ± SEM. The mean and SEM are reported in the Results section. The specific statistical test, n, what n represents, and exact F and corrected p values can be found in the figure legends.

Supplementary Material

Refer to Web version on PubMed Central for supplementary material.

Acknowledgments:

We acknowledge funding from: R01 MH100292 (NIMH), DP2 MH100011 (NIH/OD), R35 NS097306 (NIH).

REFERENCES

Agmon A, Connors BW (1991) Thalamocortical responses of mouse somatosensory (barrel) cortex in vitro. Neuroscience 41:365–379. [PubMed: 1870696]

Apkarian AV, Thomas PS, Krauss BR, Szeverenyi NM (2001) Prefrontal cortical hyperactivity in patients with sympathetically mediated chronic pain. Neurosci Lett 31:193–197.

Basbaum AI, Bautista DM, Scherrer G, and Julius D (2009) Cellular and molecular mechanisms of pain. Cell 139:267–284. [PubMed: 19837031]

Berendse HW, Groenewegen HJ (1991) Restricted cortical termination fields of the midline and intralaminar thalamic nuclei in the rat. Neuroscience 42:73–102. [PubMed: 1713657]

Bester H, Bourgeais L, Villanueva L, Besson JM, Bernard JF (1999) Differential projections to the intralaminar and gustatory thalamus from the parabrachial area: a PHA-L study in the rat. J Comp Neurol 405:421–449. [PubMed: 10098938]

Blom SM, Pfister JP, Santello M, Senn W, Nevian T (2014) Nerve injury-induced neuropathic pain causes disinhibition of the anterior cingulate cortex. J Neurosci 34:5754–5764. [PubMed: 24760836]

Bolkan SS, Stujenske JM, Parnaudeau S, et al. (2017) Thalamic projections sustain prefrontal activity during working memory maintenance. Nature Neuroscience 20(7):987–996. [PubMed: 28481349]

Bouhassira D, Lanteri-Minet M, Attal N, Laurent B, Touboul C (2008) Prevalence of chronic pain with neuropathic characteristics in the general population. Pain 136:380–387. [PubMed: 17888574]

Breivik H, Collett B, Ventafridda V, Cohen R, Gallacher D (2006) Survey of chronic pain in Europe: prevalence, impact on daily life, and treatment. Eur J Pain 10:287–333. [PubMed: 16095934]

Casey KL (1999) Forebrain mechanisms of nociception and pain: analysis through imaging. PNAS 96:7668–74. [PubMed: 10393878]

Chai S-C, Kung J-C, Shyu B-C (2010) Roles of the anterior cingulate cortex and medial thalamus in short-term and long-term aversive information processing. Mol Pain 6:1–10. [PubMed: 20089138]

Cliffer KD, Burstein R, Giesler GJ Jr (1991) Distributions of spinothalamic, spinohypothalamis, and spinotelencephalic fibers revelaed by anterograde transport of PHA-L in rats. J Neurosci 11:852–868. [PubMed: 1705972]

Delevich K, Tucciarone J, Huang ZJ, Li B (2015) The mediodorsal thalamus drives feedforward inhibition in the anterior cingulate cortex via parvalbumin interneurons. J Neurosci 35:5743–5753. [PubMed: 25855185]

Dembrow NC, Chitwood RA, Johnston D (2010) Projection-specific neuromodulation of medial prefrontal cortex neurons. J Neurosci. 30,16922–16937. [PubMed: 21159963]

Deyama S, Yamamoto J, Machida T, Tanimoto S, Nakagawa T, Kaneko S, Satoh M, Minami M (2007) Inhibition of glutamatergic transmission by morphine in the basolateral amygdaloid nucleus reduces pain-induced aversion. Neurosci Res. 59:199–204. [PubMed: 17675178]

Dong WK, Ryu H, Wagman IH (1978) Nociceptive responses of neurons in medial thalamus and their relationship to spinothalamic pathways. J Neurophysiol 41:1592–1613. [PubMed: 731292]

Fardin V, Oliveras JL, Besson JM (1984) A reinvestigation of the analgesic effects induced by stimulation of the periaqueductal gray matter in the rat. II. Differential characteristics of the analgesia induced by ventral and dorsal PAG stimulation. Brain Res 306:125–39. [PubMed: 6466968]

Fernandez E, Turk DC (1992) Sensory and affective components of pain: separation and synthesis. Psychol Bull 112:205–217. [PubMed: 1454892]

Floresco SB, Grace AA (2003) Gating of hippocampal-evoked activity in prefrontal cortical neurons by inputs from the mediodorsal thalamus and ventral tegmental area. J Neurosci 23:3930–3943. [PubMed: 12736363]

Folt EL and White LW Jr (1963) Pain “relief” by cingulotomy. J Neurosurg 19:89–100.

Gao Y-J, Ren W-H, Zhang Y-Q, Zhao Z-Q (2004) Contributions of the anterior cingulate cortex and amygdala to pain- and fear-conditioned place avoidance in rats. Pain 110:343–353. [PubMed: 15275785]

Gee S, Ellwood I, Patel T, Luongo F, Deisseroth K, Sohal SV (2012) Synaptic activity unmasks dopamine D2 receptor modulation of a specific class of layer V pyramidal neurons in prefrontal cortex. J Neurosci 32:4959–71. [PubMed: 22492051]

Giesler GJ Jr, Menetrey D, Basbaum AI (1979) Differential origins of spinothalamic tract projections to medial and lateral thalamus in the rat. J Comp Neur 184:107–126. [PubMed: 84002]

Guo ZV, Inagaki HK, Daie K, Druckmann S, Gerfen CR, Svoboda K (2017) Maintenance of persistent activity in a frontal thalamocortical loop. Nature 545:181–186. [PubMed: 28467817]

Helmstetter FJ, Bellgowan PS (1992) Lesions of the amygdala block conditional hypoalgesia on the tail flick test. Brain Res. 612:253–257.

Hoover WB, Vertes RP (2007) Anatomical analysis of afferent projections to the medial prefrontal cortex in the rat. Brain Struct Funct. 212:149–179. [PubMed: 17717690]

Hsu M-M, Kung J-C, Shyu B-C (2000) Evoked responses of the anterior cingulate cortex to stimulation of the medial thalamus. J Neurophysiol 43:81–89.

Hsu M-M, Shyu B-C (1997) Electrophysiological study of the connection between medial thalamus and anterior cingulate cortex in the rat. NeuroReport 8:2701– 2707. [PubMed: 9295104]

Hurt RW and Ballantine HT (1973) Stereotactic anterior cingulate lesions for persistent pain: a report of 68 cases. Clin Neurosurg 21:334–351.

Johansen JP, Fields HL, Manning BH (2001) The affective component of pain in rodents: direct evidence for a contribution of the anterior cingulate cortex. PNAS 98:8077–8082. [PubMed: 11416168]

Juarez-Salinas DL, Braz JM, Hamel KA, Basbaum AI (2018) Pain relief by supraspinal gabapentin requires descending noradrenergic inhibitory controls. Pain Rep 3:e659. [PubMed: 30123855]

King T, Vera-Portocarrero L, Gutierrez T, Vanderah TW, Dussor G, Lai J, Porreca F (2009) Unmasking the tonic-aversive state in neuropathic pain. Nat Neurosci 12:1364–1366. [PubMed: 19783992]

Krettek JE, Price JL (1977) The cortical projections of the mediodorsal nucleus and adjacent thalamic nuclei in the rat. J Comp Neurol 171:157–191. [PubMed: 64477]

Kuroda M, Murakami K, Oda S, Shinkai M, Kishi K (1993a) Direct synaptic connections between thalamocortical axon terminals from the mediodorsal thalamic nucleus (MD) and corticothalamic neurons to MD in the prefrontal cortex. Brain Res 612:339–344. [PubMed: 7687193]

Kuroda M, Yokofujita J, Murakami K (1998) An ultrastructural study of the neural circuit between the prefrontal cortex and the mediodorsal nucleus of the thalamus. Prog Neurobiol 54:417–458. [PubMed: 9522395]

LaGraize SC, Labuda CJ, Rutledge MA, Jackson RL, Fuchs PN (2004) Differential effect of anterior cingulate cortex lesion on mechanical hypersensitivity and escape/avoidance behavior in an animal model of neuropathic pain. Exp Neurol 188:139–148. [PubMed: 15191810]

LeDoux JE (2000) Emotion circuits in the brain. Annu Rev Neurosci. 23:155–84. [PubMed: 10845062]

Lee S, Ahmed T, Lee S, Kim H, Choi S, Kim DS, Kim SJ, Cho J, Shin HS (2011) Bidirectional modulation of fear extinction by mediodorsal thalamic firing in mice. Nat Neurosci 15:308–14. [PubMed: 22197828]

Li XB, Inoue T, Nakagawa S, Koyama T (2004) Effect of mediodorsal thalamic nucleus lesion on contextual fear conditioning in rats. Brain Res 1008:261–72. [PubMed: 15145764]

Li Z, Wang J, Chen L, Zhang M, Wan Y (2013) Basolateral amygdala lesion inhibits the development of pain chronicity in neuropathic pain rats. PLoS One 8:e70921. [PubMed: 23940666]

Mao J, Mayer JD, Price DD (1993) Patterns of increased brain activity indicative of pain in a rat model of peripheral mononeuropathy. J Neurosci 13:2689–2702. [PubMed: 8388924]

Matsumoto M, Hikosaka O (2009) Representation of negative motivational value in the primate lateral habenula. Nat Neurosci 12:77–84. [PubMed: 19043410]

Mcdonald AJ (1991) Organization of amygdaloid projections to the prefrontal cortex and associated striatum in the rat. Neuroscience 44:1–14. [PubMed: 1722886]

Melzack R, Casey KL (1968) Sensory, motivational, and central determinants of pain: a new conceptual model The skin senses (Kenshalo D Ed.), pp423.

Moisset X and Bouhassira D (2007) Brain imaging of neuropathic pain. Neuroimage 37:80–88.

Musil SY, Olson CR (1988) Organization of cortical and subcortical projections to anterior cingulate cortex in the cat. J Comp Neurol 272:203–218. [PubMed: 2456311]

Phillips EA and Hasenstaub AR (2016) Asymmetric effects of activating and inactivating cortical interneurons. Elife 10:e18383.

Pirot S, Jay TM, Glowinski J, Thierry AM (1994) Anatomical and electrophysiological evidence for an excitatory amino acid pathway from the thalamic mediodorsal nucleus to the prefrontal cortex in the rat. Eur J Neurosci 6: 1225–1234. [PubMed: 7524967]

Price DD (2000) Psychological and neural mechanisms of the affective dimension of pain. Science 288:1769–72. [PubMed: 10846154]

Qu C, King T, Okun A, Lai J, Fields H, Porecca F (2011) Lesion of the rostral anterior cingulate cortex eliminates the aversiveness of spontaneous neuropathic pain following partial or complete axotomy. Pain 152:1641–1648. [PubMed: 21474245]

Rainville P, Duncan HG, Price DD, Carrier C, Bushnell MC (1997) Pain affect encoded in human anterior cingulate but not somatosensory cortex. Science 277:968– 971. [PubMed: 9252330]

Rinaldi CP, Young FR, Albe-Fessard D, Chodakiewtiz J (1991) Spontaneous neuronal hyperactivity in the medial and intralaminar thalamic nuclei of patients with deafferentation pain. J Neurosurg 74:415–421. [PubMed: 1993906]

Sarter M, Markowitsch HJ (1983) Convergence of basolateral amygdaloid and mediodorsal thalamic projections in different areas of the frontal cortex in the rat. Brain Res Bull. 10:607–622. [PubMed: 6871734]

Schmitt LI, Wimmer RD, Nakajima M, Happ M, Mofakham S, Halassa MM (2017) Thalamic amplification of cortical connectivity sustains attentional control. Nature 545(7653):219–223. [PubMed: 28467827]

Sikes WR, Vogt AB (1992) Nociceptive neurons in Area 24 of Rabbit Cingulate Cortex. J Neurophys 68:1720–1732.

Stamatakis AM, Stuber GD (2012) Activation of lateral habenula inputs to the ventral midbrain promotes behavioral avoidance. Nat Neurosci 15,1105–1107. [PubMed: 22729176]

Swadlow HA (2002) Thalamocortical control of feed-forward inhibition in awake somatosensory “barrel” cortex. Philos Trans R Soc Lond B Biol Sci 357:1717–1727. [PubMed: 12626006]

Swadlow HA (2003) Fast-spike interneurons and feedforward inhibition in awake sensory neocortex. Cereb Cortex 13:25–32. [PubMed: 12466212]

Tanimoto S, Nakagawa T, Yamauchi Y, Minami M, Satoh M (2003) Differential contributions of the basolateral and central nuclei of the amygdala in the negative affective component of chemical somatic and visceral pains in rats. Eur J Neurosci. 18:2343–2350. [PubMed: 14622196]

Tracey I and Mantyh WP (2007) The cerebral signature for pain perception and its modulation. Neuron 55:377–391. [PubMed: 17678852]

Treede RD, Kenshalo DR, Gracely RH, Jones AK (1999) The cortical representation of pain. Pain 79:105–111. [PubMed: 10068155]

Urban R, Scherrer G, Goulding EH, Tecott LH, Basbaum AI (2011) Behavioral indices of ongoing pain are largely unchanged in male mice with tissue or nerve injury-induced mechanical hypersensitivity. Pain 152:990–1000. [PubMed: 21256675]

Velayos JL, Suarez-Reinoso F (1985) Prosencephalic afferents to the mediodorsal thalamic nucleus. J Comp.Neurol. 242:161–181. [PubMed: 4086663]

Villanueva L, Cliffer KD, Sorkin LS, Le Bars D, Willis WD Jr (1990) Convergence of heterotopic nociceptive information onto neurons of caudal medullary reticular formation in monkey. J Neurophsiol 63:1118–1127.

Villanueva L, Debois C, Le Bars D, Bernard JF (1998) Organization of diencephalic projections from the medullary sbunucleus reticularis dorsalis: a retrograde and anterograde tracer study in the rat. J Comp Neurol 390:133–160. [PubMed: 9456181]

Vogt BA (2005) Pain and emotion interactions in subregions of the cingulate gyrus. Nature Reviews Neuroscience 6:533–544. [PubMed: 15995724]

Wang H-C, Chai S-C, Wu Y-S, Wang C-C (2007) Does the medial thalamus play a role in the negative affective component of visceral pain in rats?. Neuroscience Letters 420:80–84. [PubMed: 17512660]

Whitt JL, Masri R, Pulimood NS, Keller A (2013) Pathological activity in mediodorsal thalamus of rats with spinal cord injury pain. J Neurosci 33:3915–3926. [PubMed: 23447602]

Yamamura H, Iwata K, Tsuboi Y, Toda K, Kitajima K, Shimizu N, Nomura H, Hibiya J, Fujita S, Sumino R (1996) Morphological and electrophysiological properties of ACC nociceptive neurons in rats. Brain Res 735:83–92. [PubMed: 8905172]

Yang J-W, Shih H-C, Shyu B-C (2006) Intracortical circuits in rat anteriorcingulate cortex are activated by nociceptive inputs mediated by the medial thalamus. J Neurophysiol 96:3409–3422. [PubMed: 16956990]

Young RF, Chambi VI (1987) Pain relief by electrical stimulation of the periaqueductal and periventricular gray matter: Evidence for a non-opioid mechanism. J Neurosurg 66:364–71. [PubMed: 3493333]

HIGHLIGHTS

- Activating MD thalamus-ACC inputs exacerbates pain-related aversion
- In pain, MD inputs to subcortically-projecting ACC neurons shift towards inhibition
- Inhibiting subcortically-projecting ACC neurons exacerbates pain-related aversion
- Unlike MD-ACC input, BLA-ACC input is strengthened in pain and mitigates aversion

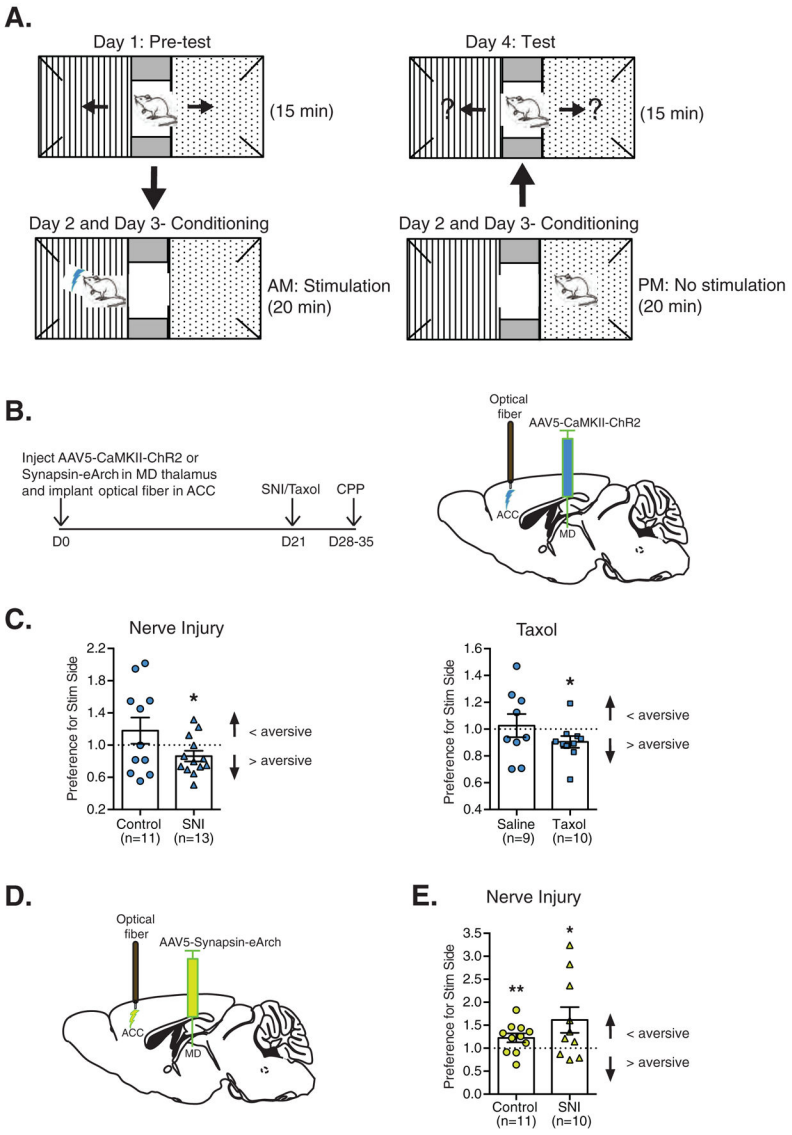

Figure 1: Activating MD-ACC input exacerbates pain-related aversion, but has no effect on animals without pain.

A. Conditioned Place Preference (CPP) Paradigm.

B. (Left) Experimental timeline. (Right) AAV5-CaMKII-ChR2-eYFP injection in MD and optical fiber implant in ACC.

C. Preference for Stim Side quantifies the ratio of time spent in the stimulated chamber on the Test vs. Pre-test day. Scores >1 or <1 indicate that stimulation reduces or exacerbates aversion (< aversive or > aversive), respectively. SNI (n = 13, $t_{(24)} = 2.09$, p = 0.048) and Taxol (n = 10, $t_{(18)} = 2.17$, p = 0.044) animals have Preference scores significantly <1 (*, p < 0.05 by unpaired t-test), i.e., they avoid the side paired with stimulation of MD inputs. Preference scores of Control (n = 11, $t_{(20)} = 1.10$, p = 0.28) and Saline animals (n = 9, $t_{(16)} = 0.30$, p = 0.77) animals are not significantly different from 1. Data are shown as mean ± SEM.

D. AAV5-Synapsin-Arch-eYFP injection in MD and optical fiber implant in ACC.

E. Quantification of Preference for Stim Side. Control animals (n = 11, $t_{(20)} = 2.29$, p = 0.033) and SNI animals (n = 10, $t_{(18)} = 2.19$, p = 0.042) have Preference scores significantly > 1 (*, $p < 0.05$ by unpaired t-test), indicating that both groups prefer the side paired with inhibition of MD inputs. The preference scores of Control and SNI animals are not statistically significantly different from each other. Data are shown as mean ± SEM. See also Figure S1A–B, S2A and S8.

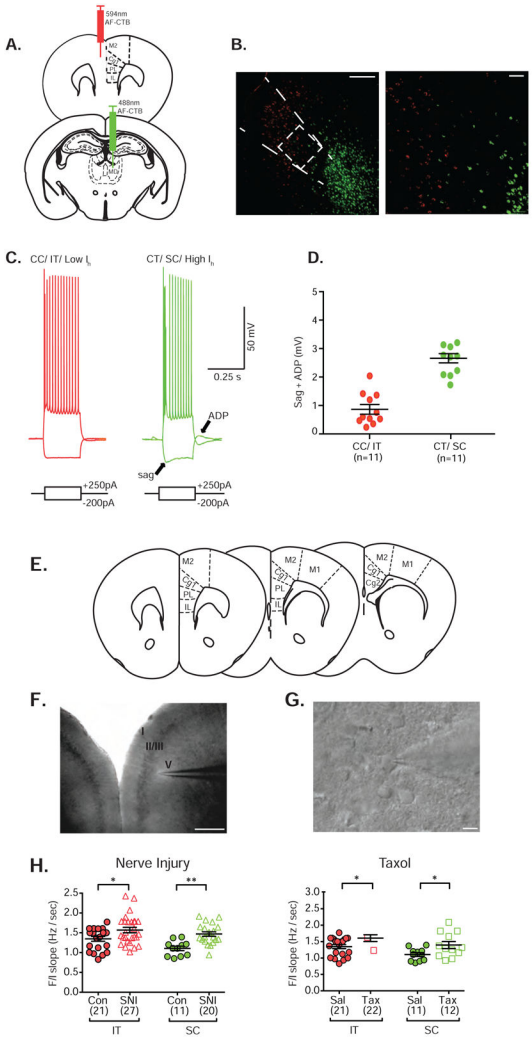

Figure 2: IT and SC neurons in layer V of ACC are hyperexcitable in SNI and Taxol animals.

A. Schematic of AF-CTB injections in the contralateral cortex or mediodorsal thalamus to label intratelencephalic (IT) and subcortical (SC) projecting cells, respectively.

B. (Left) Low power image of retrogradely labeled IT (red) and SC cells (green) in Cg1/ ACC. Midline and the layers are demarcated. Scale bar = 50 μm. (Right) High power image of inset shows overlap of IT and SC cells in Cg1/ACC. Scale bar = 10 μm.

C. Sample responses of labeled IT and SC neurons to hyperpolarizing or depolarizing current injection. The voltage sag and rebound after-depolarization (ADP) in response to hyperpolarizing current injection is evident in the SC neuron, but not the IT neuron (arrows).

D. The magnitude of h-current, measured as the sum of the voltage sag and rebound afterdepolarization, in response to hyperpolarizing current pulses in IT and SC neurons. Numbers of cells are indicated in parentheses. Data are shown as mean ± SEM.

E. Top: Representative coronal sections from Bregma 1.48 mm to Bregma 1.18 mm including ACC (Cg1 and Cg2).

F. DIC image of patch pipette in layer V of ACC. Scale bar = 50 μm.

G. 40X DIC image of whole-cell patch clamp recording. Scale bar = 10 μm.

H. The F/I slope (Hz/pA) was significantly increased in both cell types from SNI (n = 3 animals) and Taxol (Tax) (n = 3 animals) compared to Controls (n = 3 animals). The number of cells for each experiment is indicated in parentheses. (Control IT cells n = 21, SNI IT cells n = 27, $t_{(46)} = 2.31$, p = 0.025; Control SC cells n = 11, SNI SC cells n = 20, $t_{(29)} = 4.07$, p = 0.0003; Saline IT cells n = 21, Taxol IT cells n = 22, $t_{(41)} = 2.14$, p = 0.039; Saline SC cells n = 11, Taxol SC cells n = 12, $t_{(21)} = 2.33$, p = 0.030). *, $p < 0.05$; **, $p < 0.01$ by unpaired t-test. Data are shown as mean ± SEM.
See also Figure S3.

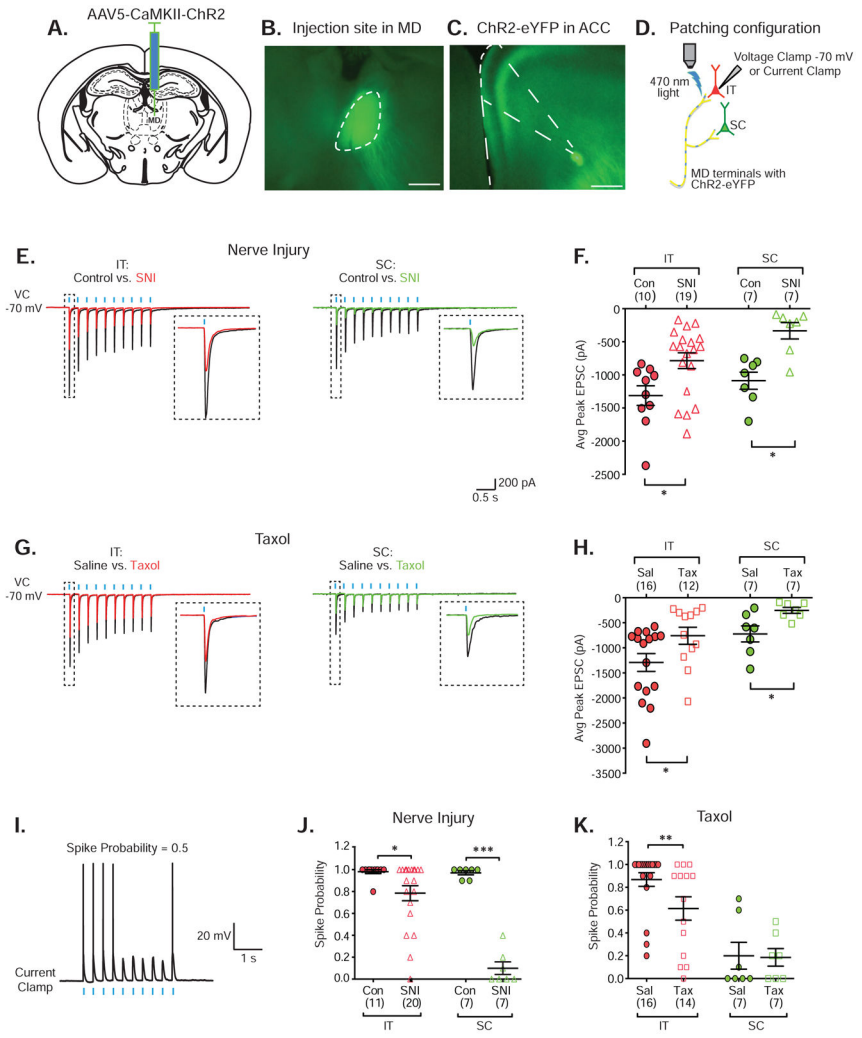

Figure 3: Excitatory responses of layer V ACC pyramidal neurons to MD inputs become weaker in SNI and Taxol animals

A. Coronal section of a mouse brain at Bregma −1.70 mm shows the site of AAV5-CaMKII-ChR2-eYFP injection in the MD thalamus.

B. Fluorescent labeling of the targeted MD. “3v” = 3rd ventricle. Scale bar = 50 μm.

C. ChR2-eYFP expression in layers I and V of ACC.

D. Schematic: configuration for recording EPSCs in IT and SC cells in response to activation of ChR2 in MD terminals (yellow).

E and G. Population average of EPSCs (voltage clamp responses at −70 mV) to 5 Hz trains of 1 ms light pulses recorded from IT and SC cells in SNI (n = 4 animals) vs. Control (n = 4 animals) and Taxol (n = 3 animals) vs. Saline (n = 3 animals). A zoom-in of the first light-evoked response is shown in the insets.

F and H. The amplitude of the first EPSC during 5, 10, or 20 Hz trains was averaged to calculate the peak EPSC amplitude for IT or SC cells (number of cells for each experiment shown in parentheses) from SNI or Taxol animals compared to Control or Saline, respectively (Control IT cells n = 10, SNI IT cells n = 19, $t_{(27)} = 2.68$, $p = 0.013$; Control SC cells n = 7, SNI SC cells n = 7, $t_{(12)} = 4.22$, $p = 0.0012$; Saline IT cells n = 16, Taxol IT cells

n = 12, $t_{(26)}$ = 2.12, p = 0.044; Saline SC cells n = 7, Taxol SC cells n = 7, $t_{(12)}$ = 2.75, p = 0.018). *, p < 0.05 by unpaired t-test. Data are shown as mean ± SEM.

I. Example current clamp responses. Spike probability = the number of light pulses that evoked spikes divided by the total number of light pulses.

J and K. Quantification of spiking in IT or SC cells (number of cells in parentheses) in response to optogenetic stimulation of MD inputs in SNI (n = 4 animals) vs. Control (n = 4 animals) and Taxol (n = 3 animals) vs. Saline (n = 3 animals). (Control IT cells n = 11, SNI IT cells n = 20, $t_{(29)}$ = 0.045; Control SC cells n = 7, SNI SC cells n = 7, $t_{(12)}$ = 14.38, p < 0.0001; Saline IT cells n = 16, Taxol IT cells n =14, $t_{(31)}$ = 2.27, p = 0.031). *, p < 0.05, ***, p < 0.001 by unpaired t-test. Data are shown as mean ± SEM. Two-way ANOVA, F(1,38) = 7.1 for a significant effect of cell type (SC vs. IT).

See also Figure S4.

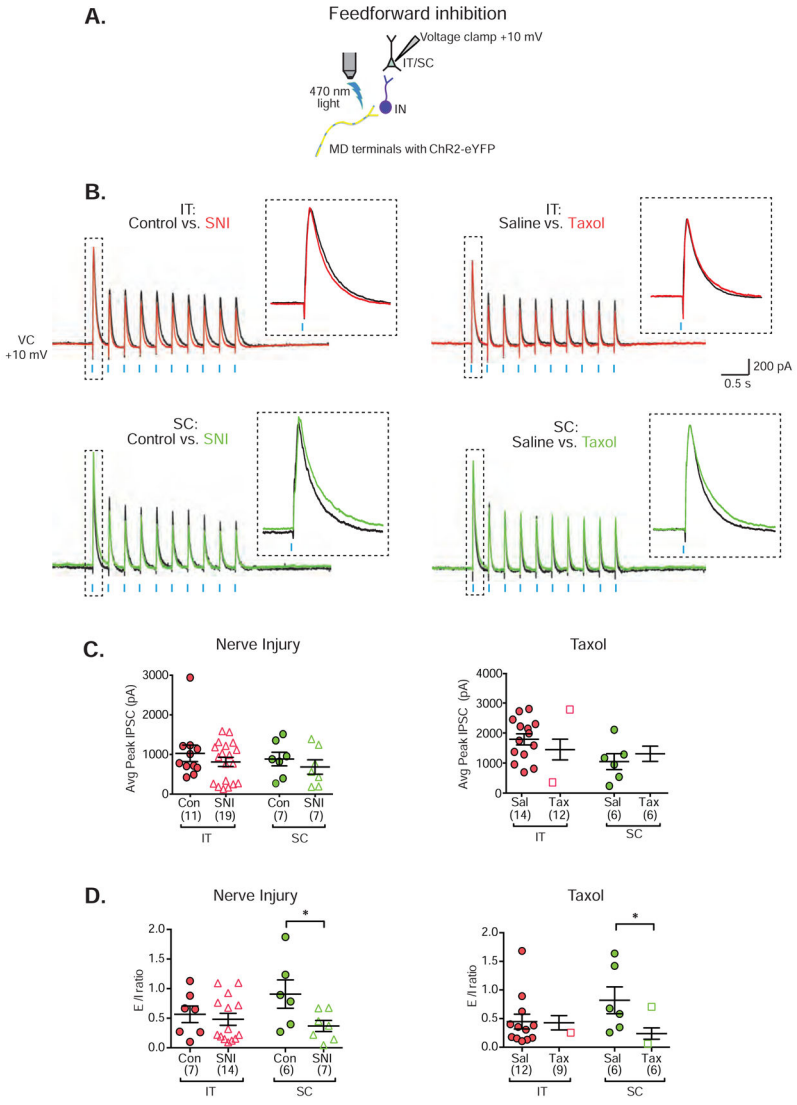

Figure 4: In SC neurons, the E/I ratio evoked by MD input shifts towards inhibition in the setting of pain.

A. Schematic of patching configuration to record feedforward inhibition evoked by MD inputs in IT or SC neurons.

B. Population average of inhibitory postsynaptic currents (IPSCs) evoked by 5 Hz trains of 5 ms light pulses, recorded in voltage clamp at +10 mV from IT or SC cells. A zoom in of the first light-evoked response is shown in the insets.

C. Quantification of peak IPSC amplitude recorded in voltage clamp at +10 mV from IT and SC cells (number of cells indicated in parentheses) in SNI (n = 4 mice) vs. control mice (n = 4) and Taxol (n = 3) vs. saline-treated mice (n = 3). Data are shown as mean ± SEM.

D. The area under the curve (AUC) for EPSCs and IPSCs (recorded in voltage clamp at −70 or +10 mV, respectively) was calculated for responses to 10 stimuli delivered at 5 Hz. In each case, we plotted the ratio of the excitatory to inhibitory AUC (E/I) for all IT and SC neurons in SNI or Taxol vs. control. *, $p < 0.05$ using two-way ANOVA. Significant main effect of condition, $p = 0.013$, and interaction between condition and cell type, $p = 0.041$,

ANOVA using pain vs. control, SNI vs. Taxol models, and cell type as factors. ANOVA run separately on SC data, using pain vs. control, SNI vs. Taxol as factors, there is a main effect of condition ($F_{(1,22)} = 5.43$, $p = 0.029$). ANOVA run separately on IT data, using pain vs. control, SNI vs. Taxol as factors indicates no effect of condition ($F_{(1,42)} = 0.05$, $p = 0.816$). Data are shown as mean ± SEM.

See also Figure S5.

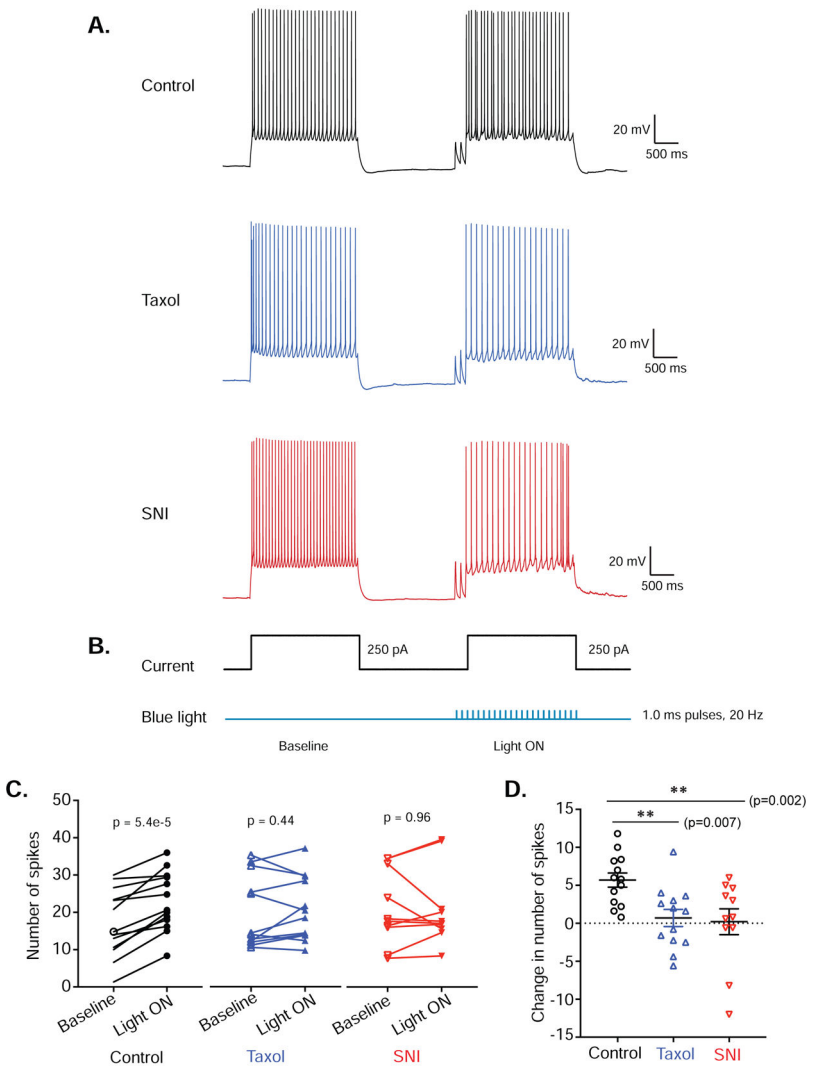

Figure 5: Optogenetic activation of MD inputs increases spiking for SC neurons in control animals but not in animals with pain.

A. Example traces showing spiking of SC neurons from Control (n = 3 mice; top), Taxol (n = 3 mice; middle), or SNI (n = 3 mice; bottom) in response to depolarizing current injection with or without concomitant optogenetic stimulation of MD input.

B. Traces showing the current pulse +/− optogenetic stimulation protocol.

C. Number of spikes in SC cells from Control (black circles), Taxol (blue, inverted triangles), or SNI (red triangles) plotted for Baseline and Light ON. There was a significant increase in spiking for Control cells (n=13) in the Light ON condition compared to Baseline ($t_{(12)}$ = 6.09, p = 0.000053, paired t-test). There is not a significant difference in the number of spikes in the Light ON condition compared to Baseline in either SNI (n = 11 cells, $t_{(9)}$ = 0.04, p =0.96, paired t-test) or Taxol (n = 13 cells, $t_{(11)}$ = 0.78, p = 0.44, paired t-test).

D. Change in the number of spikes between Baseline and Light ON plotted for Control (black circles), Taxol (blue, inverted triangles) and SNI (red triangles). There is a significant difference between Control vs. SNI ($t_{(22)}$ = 2.9, p = 0.007, unpaired t-test) and Control vs. Taxol ($t_{(23)}$ = 3.4, p = 0.002, unpaired t-test).

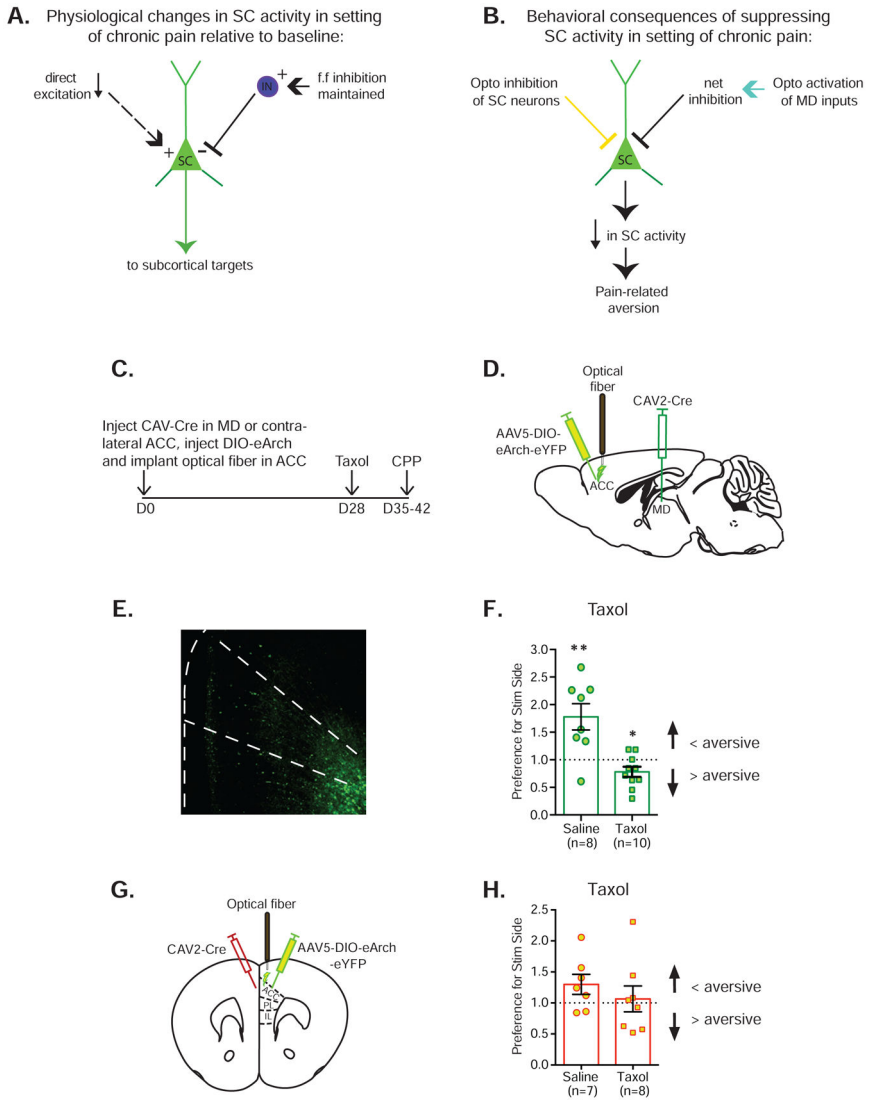

Figure 6: Optogenetic inhibition of SC neurons in ACC exacerbates pain-related aversion.

A. Schematic: in the setting of chronic pain, the direct excitation of SC neurons in ACC evoked by MD input is significantly reduced, compared to control conditions (indicated by dashed arrow and smaller '+'). By contrast, feedforward (f.f.) inhibition is maintained (indicated by solid line and '−' symbol).

B. In the setting of chronic pain, optogenetically activating ('opto activation', blue arrow) MD-ACC inputs results in a shift of the E/I ratio in SC neurons towards inhibition ('net inhibition') and a reduction in SC neuron activity. Based on this, direct optogenetic inhibition ('opto inhibition', yellow arrow) of SC neurons should elicit similar effects, e.g., pain-related aversion.

C. Experimental timeline.

D. Injection of CAV2-Cre in MD thalamus and AAV5-DIO-eArch-eYFP into ACC, and implantation of an optical fiber over ACC, to target SC neurons in ACC.

E. Sparse labeling of SC neurons with eYFP in layers V and VI of ACC.

F. Quantification of Preference for Stim Side of saline injected and Taxol injected animals. For Taxol animals, the preference for the side paired with optogenetic inhibition of SC neurons is significantly < 1 (n =10 animals, $t_{(18)} = 2.37$, p = 0.030, *, p < 0.05 by unpaired t-test), indicating that inhibition of SC neurons elicits aversion in animals with chronic neuropathic pain. In contrast, the Preference score in Saline animals is significantly > 1 (n = 8 animals, $t_{(14)} = 3.28$, p = 0.0055, **, p < 0.01 by unpaired t-test). Data are represented as mean ± SEM.

G. Injection of CAV2-Cre in contralateral ACC and AAV5-DIO-eArch-eYFP and implantation of an optical fiber over ipsilateral ACC, to target IT neurons in ACC.

H. Quantification of Preference for Stim Side. The preference score of Saline and Taxol animals is not significantly different from 1 (Saline, n = 7, $t_{(12)} = 1.86$, p = 0.088; Taxol, n = 8, $t_{(14)} = 0.32$, p = 0.76, unpaired t-test). Data are represented as mean ± SEM.

See also Figure S1F–H, Figure S6 and S8.

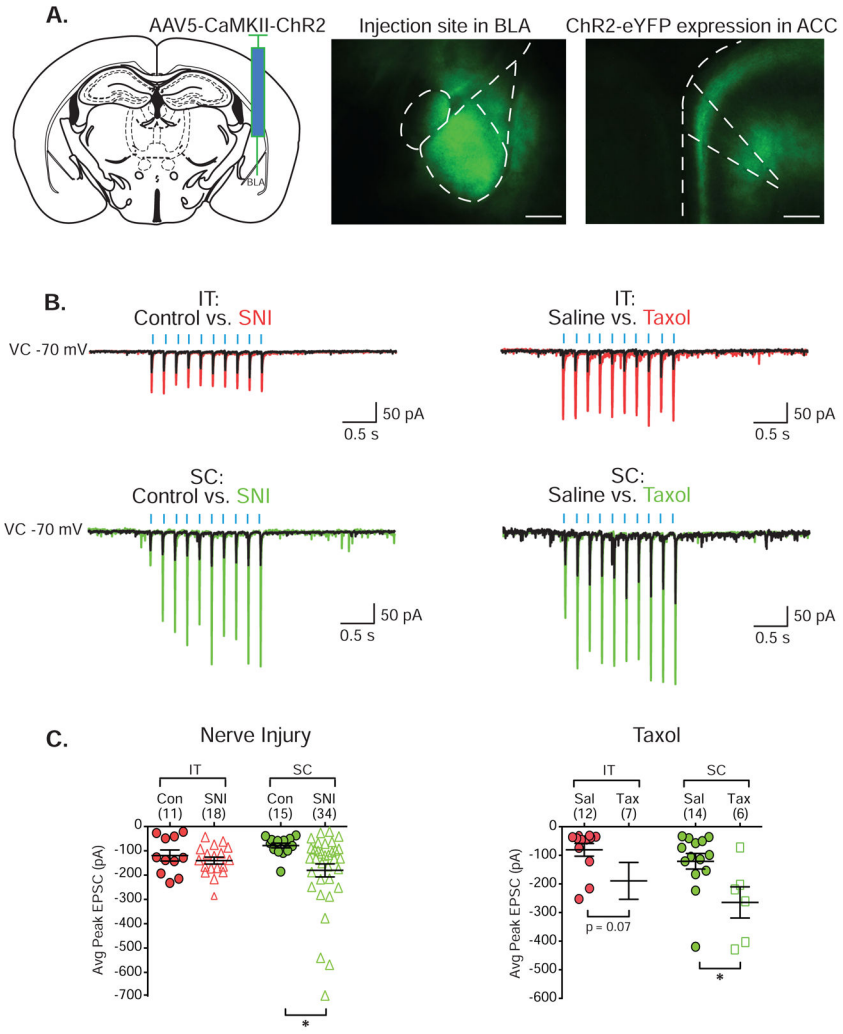

Figure 7: Excitatory synaptic responses evoked by BLA inputs in layer V ACC neurons are significantly increased in SNI and Taxol animals.

A. (Left) Coronal section of a mouse brain at Bregma −1.34 mm showing injection of AAV5-CaMKII-ChR2-eYFP into BLA. (Middle) Representative low power image shows ChR2-eYFP expression in the targeted BLA. LA: lateral amygdala; CeA: central amygdala. (Right) Low power image of ChR2-eYFP expression in layer V of ACC. Scale bar = 50 μm.

B. Population average of EPSCs (voltage clamp responses at −70 mV) to 5 Hz trains of 1ms light pulses recorded from IT or SC cells in SNI (n = 4 mice) vs. control mice (n = 4) and Taxol (n = 3) vs. Saline-treated mice (n = 4).

C. Amplitudes of the first EPSCs in 5, 10, or 20 Hz trains were averaged to calculate the peak EPSC amplitude for each IT or SC cells in SNI or Taxol animals (number of cells indicated in parentheses) compared to Control or Saline. (Control IT cells n = 11, SNI IT cells n = 18, $t_{(27)} = 0.82$, p = 0.42; Control SC cells n = 15, SNI SC cells n = 34, $t_{(47)} = 2.48$, p = 0.017; Saline IT cells n = 12, Taxol IT cells n = 7, $t_{(17)} = 1.93$, p = 0.071; Saline SC cells n = 14, Taxol SC cells n = 6, $t_{(18)} = 2.63$, p = 0.017) *, $p < 0.05$ by unpaired t-test. Data are shown as mean ± SEM.

See also Figure S7.

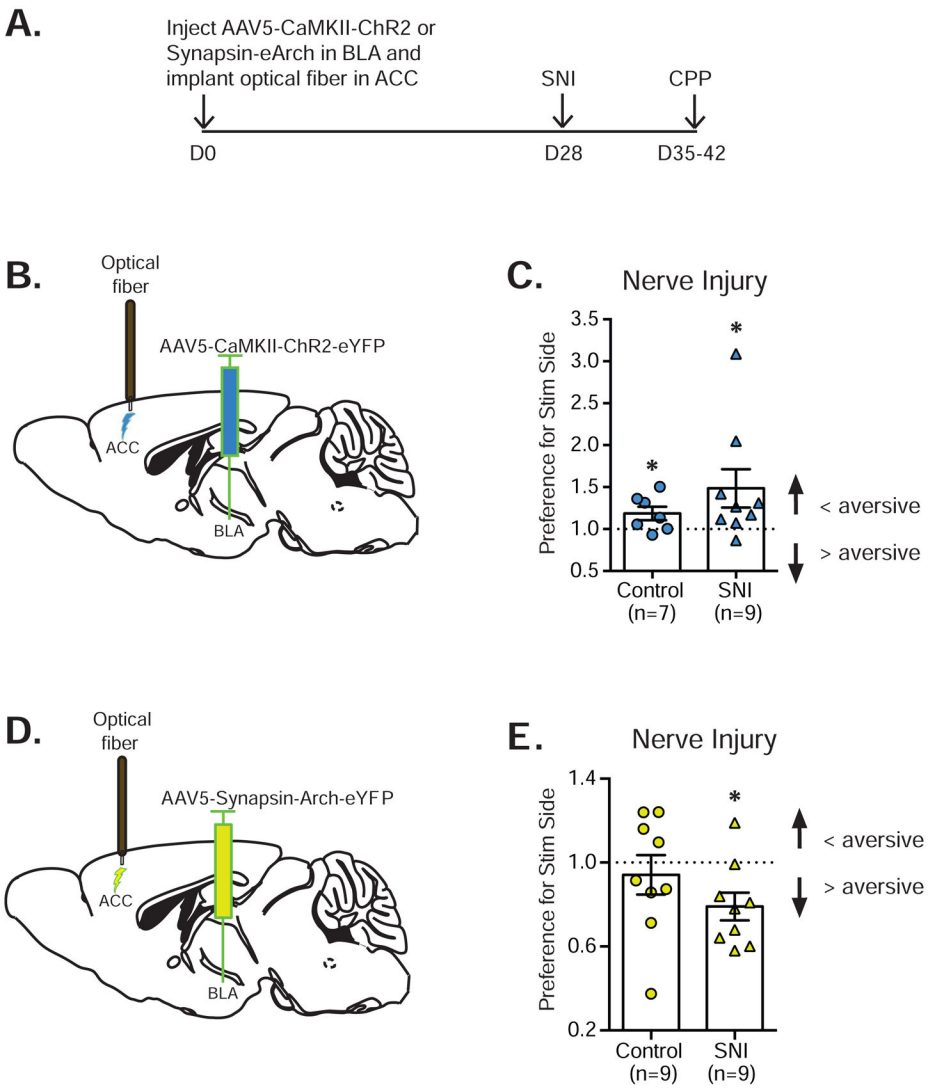

Figure 8: Inhibiting BLA-ACC inputs elicits aversion in animals with pain.

A. Experimental timeline.

B. AAV5-CaMKII ChR2-eYFP injection in BLA and optical fiber in ACC.

C. Quantification of Preference for Stim Side. Control animals (n = 7, $t_{(12)} = 2.35$, p = 0.037) and SNI animals (n = 9, $t_{(16)} = 2.13$, p = 0.049) have Preference scores significantly > 1 (*, $p \leq 0.05$ by unpaired t-test). Data are shown as mean ± SEM.

D. AAV5-Syn-eArch-eYFP injection in BLA and optical fiber in ACC.

E. Quantification of Preference for Stim Side. SNI animals (n = 9, $t_{(16)} = 3.16$, p = 0.0061) have preference scores significantly < 1 (**, $p < 0.01$ by unpaired t-test.), i.e., they avoid the side paired with optogenetic inhibition of BLA inputs. Preference score of control animals (n = 9, $t_{(16)} = 0.63$, p = 0.54) is not significantly different from 1. Data are shown as mean ± SEM.

See also Figure S1D–E, S2B and S8.